Low Cost Electronically Steered Antenna and Receiver System for Mobile Satellite Communications

José I. Alonso, *Member, IEEE,* José M. Blas, Luis E. García, *Student Member, IEEE,* Javier Ramos, *Student Member, IEEE,* Jesús de Pablos, Jesús Grajal, Gian G. Gentili, *Member, IEEE,* Javier Gismero, and Félix Pérez, *Member, IEEE*

***Abstract*— The design, construction, and basic characteristics of an electronically steered, adaptive phased array antenna for land mobile satellite communications are described here. The antenna system includes an array of six microstrip stacked patch antennas, each one connected to an RF channel, which include a monolithic microwave/millimeter wave integrated circuit (MMIC) low noise amplifier and a commercial silicon monolithic I-Q modulator. A six-way microstrip combiner adds the six channels so that the resulting signal is introduced in a global positioning system (GPS) receiver, constructed with two commercial application specific integrated circuits (ASIC's). This receiver has a PC interface which include control boards, specifically designed for this application, that allow the setting of the amplitude and phase of each RF channel. Acquisition and tracking algorithms have been programmed in C-language for working in real time using as input data the signal levels provided by the receiver.**

I. Introduction

NOWADAYS, the potential market for mobile communications and navigation systems based on satellites has triggered the development of a wide range of future integrated communications and navigation systems, like INMARSAT-21, IRIDIUM, GLOBALSTAR, ODYSSEY, and GPS as well [1]. Whether geostationary satellites are employed or not, the satellite-vehicle link needs a directional antenna, which becomes a critical component in the mobile system. The directional beam must be dynamically oriented toward the satellite and thus mobility and use easiness could be not limited. Several satellite-tracking mobile vehicular antenna systems, at different frequency bands, have been developed [2], [3]. Also, a number of techniques aimed at minimizing the cost of such arrays without significantly sacrificing performance have been considered. On the other hand, there is currently a considerable interest in the use of adaptive array antennas for applications in the field of mobile satellite communications [4]–[6], because they offer advantages over conventional fixed pattern antennas, like the ability of changing the terrestrial position where the communication is made and the beam shape conformation to the actual requirements of the transmission or reception.

A new vehicle-mounted adaptive electronically steered array has been designed, developed and manufactured. The aim has been to obtain a system that allows realizing experiments in order to evaluate a possible solution for the mobile antenna segment of a mobile satellite communications system. Another important point is to gather experience in order to develop technology and make possible more advanced antennas, which will increase the benefit of introducing adaptive antennas in this kind of systems.

The global positioning system (GPS) has been used due to the following reasons: availability of cheap and small commercial receivers and easiness of distinguish a given satellite signal among the others, which is very useful for test purposes. In fact, it can be detected and used like the pilot signal of INMARSAT. There is even an additional advantage: the fact that GPS receivers supply satellite positions. This helps to calibrate and evaluate the whole system.

This paper presents the design and mechanical characteristics of the planar array and RF subsystem of the adaptive antenna, together with the design of GPS commercial receiver and the antenna tracking control system needed to make the main beam scan for satellites and track them into the space. The system also includes several algorithms to maximize the received signal in urban environment. Fig. 1 shows a block diagram of the developed adaptive antenna system.

II. System Description

A. Array Antenna Design

A six-element array was developed using the stacked square patch described below. Each patch was placed in the corner of a regular hexagon of side equal to 10.6 cm ($0.55\lambda_0$ for $f = 1.558$ Ghz). Two orthogonal probes were used to connect the patch to the inputs of a 3 dB-90° hybrid, in order to receive circularly polarized waves. The output of the hybrid is followed by a MMIC low noise amplifier (LNA), specifically developed for this application.

Manuscript received April 1, 1996. This work was supported in part by the Spanish National Board of Scientific and Technological Research (CICYT) under project TIC93-0055-C03-01 and the Consejería de Educación y Cultura de la Comunidad de Madrid with research grants provided to some of the authors.

J. I. Alonso, J. M. Blas, L. E. Garcia, J. Ramos, J. de Pablos, J. Grajal, J. Gismero, and F. Pérez are with the Departamento Señales, Sistemas y Radiocomunicaciones, E.T.S.I. Telecomunicacion, U.P.M. Ciudad Universitaria, s/n 28040 Madrid, Spain.

G. Gentili is with the Dipartimento di Elettronica e Informazione, Politecnico di Milano, 20133 Milano, Italy.

Publisher Item Identifier S 0018-9480(96)08563-8.

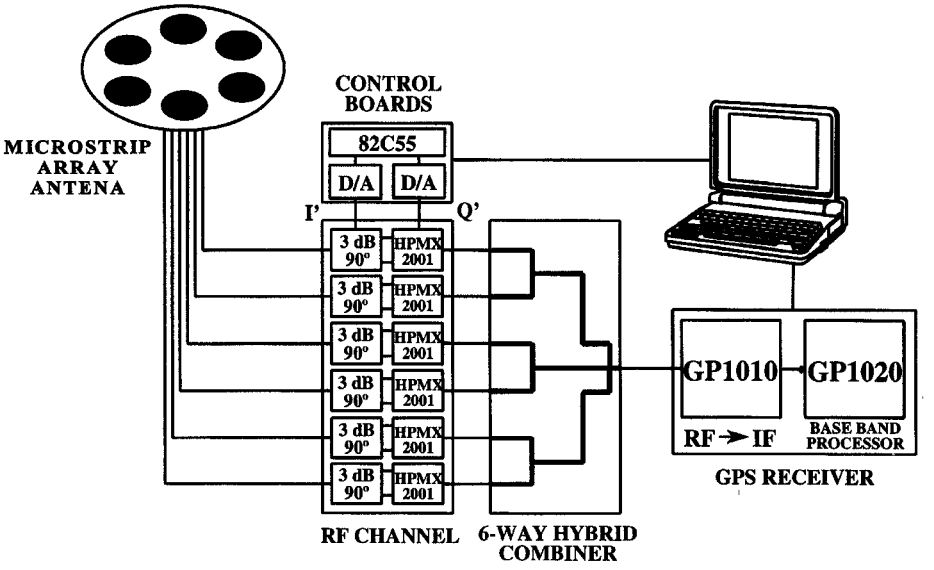

Fig. 1. Block diagram of the electronically steered antenna.

The designed array has a frequency range of 1440–1660 MHz, appropriate for mobile satellite services. Furthermore, it can be electronically steered in a practical scan volume with 90° elevation and 360° azimuth. The antenna has been designed to produce a gain between 10 and 12 dBic. The hexagon side of the array antenna is 20 cm.

1) Stacked Microstrip Patch Array Element: Microstrip antennas have proved to be adequate for mobile communications due to their many advantages, such as low profile and weight, easy integration with printed circuits (both in monolithic and hybrid technologies), photolithographic process of fabrication, etc., [7], [8]. However, due to their resonant behavior, they radiate efficiently only over a narrow frequency band, with bandwidths typically of a few percent (2%–3% for moderate substrate heights) [7]. A better way to improve the narrow bandwidth of the conventional patch antenna involves adapting the input impedance knowing that the bandwidth of the radiation pattern is higher than that of the input impedance. This can be done with a conventional impedance matching circuit network or adding parasitic elements electromagnetically coupled to the driven patch. Parasitic elements can be placed coplanar to the driven patch in different configurations [9] or stacked [10]. The later configuration has been chosen for the array elements because of its symmetry and it does not need additional space on the plane of the array. In addition, input impedance behavior can be easily modified by changing the separation between the upper and lower patches. Thus the bandwidth of the antenna can be adjusted, also offering the possibility of dual frequency operation.

A computer code based on a rigorous Green's function technique has been developed to help in the array antenna design process. The program developed is capable of analyzing single and stacked rectangular microstrip patch antennas residing in a metallic cavity [11]. This configuration can be useful in the design of arrays with low interelements couplings [12], leading to larger scan volumes with respect to the case of patches on an infinite substrate [13]. By using a large cavity size and avoiding the excitation of spurious surface waves we verified that the program yields useful information also for the design of arrays of coaxial-fed single and stacked rectangular patch antennas in an open environment. Besides the computation of input impedance, the modeling of the rectangular stacked patch antennas has allowed obtaining information on bandwidth, radiation pattern, and parasitic coupling between the array elements. This last effect is particularly important in the case of stacked patch antennas, since the parasitic patch couples the adjacent array element in a more relevant and complex way. A moment-method approach has been used, based on a suitable dyadic Green's function for the external and internal problems. The integral equation which is obtained by imposing the continuity of tangential electric and magnetic fields is then solved by Galerkin's method. The external problem makes use of the well-known free-space dyadic Green's function of the admittance type, yielding the magnetic field generated by a magnetic current sheet. For the internal problem a TE/TM waveguide mode expansion of Green's dyad has been used. Although the derivation of such a functions is straightforward, owing to the slow convergence of modal series, the numerical computations are very cumbersome, and it seemed necessary to look for alternative Green's function representations with improved convergence properties. By identifying the asymptotic behavior of Green's dyad and by using a multiple image extraction, one gets to a form which is very suitable for the computation since it comprises a fast converging frequency dependent part plus a frequency independent image series. This represents the asymptotic behavior of the TE part of Green's dyad. The radiation pattern is computed by a standard Fourier-transform of the aperture field. Coupling between elements is computed by placing two or more coaxial feeds (modeled as current probes) and by obtaining the scattering matrix from the impedance matrix. This last is obtained directly with the formulation used. A more detailed description of the developed technique can be found in [14].

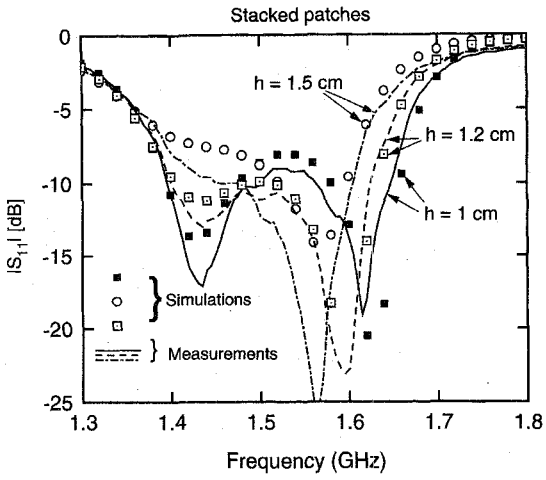

Fig. 2. Input reflection coefficient of the stacked patch element for different thicknesses of the foam layer.

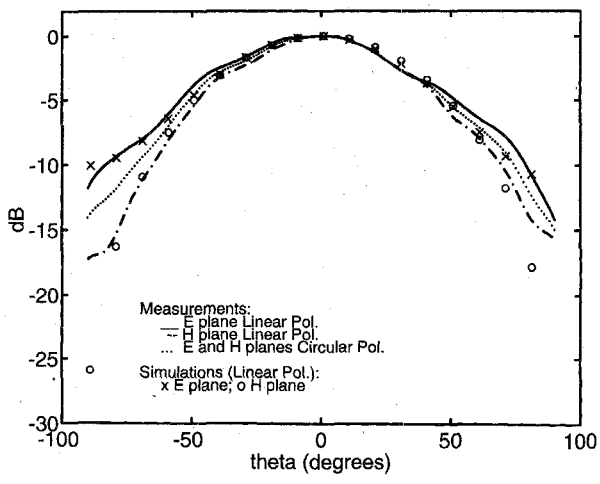

Fig. 3. Radiation patterns of the stacked patch element with 15 mm thick foam.

Employing the code described above, a stacked patch has been designed. It consists of square upper and lower patches of side 6.62 cm and impressed on a CuClad substrate of ϵ_r of 2.17 and $h = 3.175$ mm. The two coaxial probes are placed 24.75 mm from the center of the patch. The separation between the upper and lower patches is provided by placing a foam between them. The foam is ROHACELL31, very similar electrically to air ($\epsilon_r = 1.01$), but rigid enough to provide consistency to the structure. Varying the thickness of this foam layer varies the separation between the lower and upper patches, so the coupling between them and the input impedance. Fig. 2 shows the measured and simulated input reflection coefficient of the stacked patch versus frequency for different thicknesses of the foam layer. The partial disagreement between measurements and simulations can be explained by observing the measurements that refer to a structure on a finite-size multilayered substrate with no cavity walls, while in the simulations the structure is considered embedded in a cavity. Although a large cavity size was used in the simulation, the two structures are not identical due to the effect of the proximity of the cavity. This effect is more noticeable when

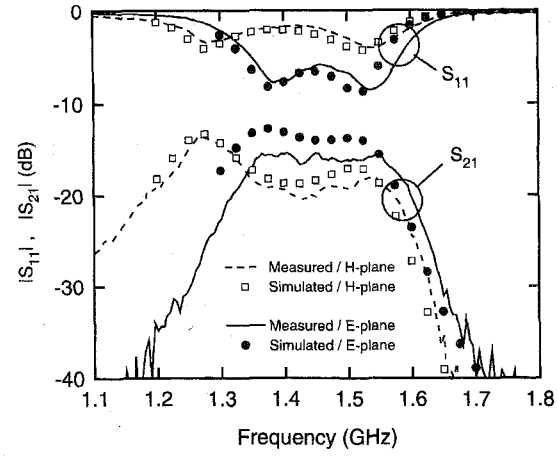

Fig. 4. Coupling between stacked patches enclosed in the same cavity and separated $\lambda_o/2$. Foam thickness: 18 mm.

the substrate height increases. Note that the main cause of disagreement between measurements and simulations is the matching level, which in the measurements is about 2 dB below that value was obtained in the simulations. It can be observed how wider bandwidths correspond to higher foam thicknesses, up to a certain limit. Bandwidths up to 230 Mhz (SWR $= 2:1$) have been observed for the present design.

Radiation patterns were also measured in an anechoic chamber. Fig. 3 shows the E-plane and H-plane normalized measured radiation patterns for both linear and circular polarization. The linear polarization pattern corresponds to one of the two orthogonal entries of the stacked antenna. The circular polarization pattern is obtained from the combination of the two orthogonal entries with a 90° phase shift, combining the E-plane of one of the linear polarization entries and the H-plane of the other entry. Also, computed results are presented in the figure. Good agreement is observed; the differences for low elevations are due to the effect of the finite ground plane of the real antenna. The small ripple in the measurement curves is due to reflections in the anechoic chamber because of the proximity of the working frequency of the antenna to the frequency lower limit of the chamber (1 GHz). Although not observable in Fig. 3, small asymmetry in the E-plane pattern (linear polarization) has been detected due to the asymmetry of the feeding. The directivity of the stacked antenna goes from 8 dB to 9 dB over the working frequency band because of the increment of the electric aperture of the antenna with the frequency. Directivity of the stacked antenna is higher than the conventional patch due to the director effect of the upper patch. The measured efficiency was around 65% and the crosspolar components below -20 dB.

Coupling between patches in single and stacked configuration has also been also simulated and measured. An example is shown in Fig. 4. The figure shows the effect of coupling for two stacked patches placed in the same cavity. One can note that the programme is capable of predicting the coupling level in E-plane and H-plane with satisfactory accuracy. A detailed explanation of the coupling mechanisms is described in [14].

2) Array Antenna: The lower substrates of the stacked patches are placed in grooves made in a hexagonal metallic

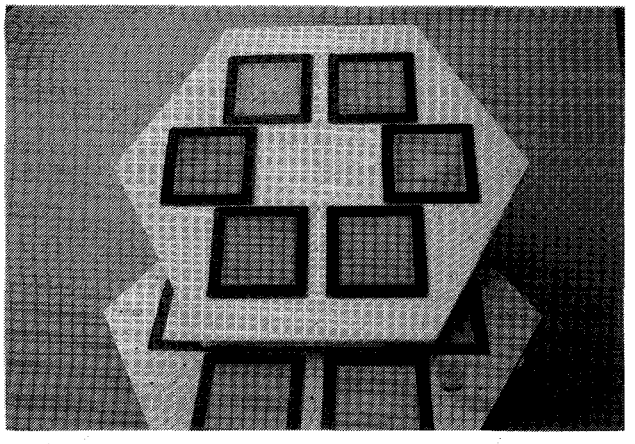

Fig. 5. Array antenna structure with upper and lower patches.

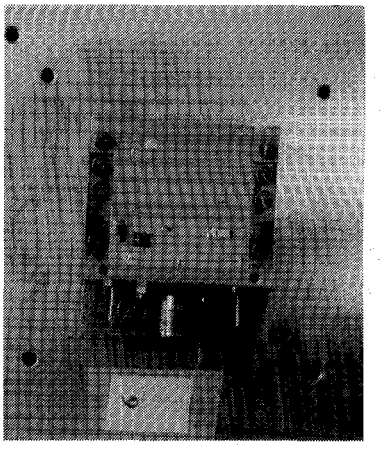

Fig. 6. Assembly of 3 dB-90° hybrid and monolithic LNA.

plate. On the other hand, the upper substrates are situated in grooves made on a foam layer. A photograph of the metallic plate and the foam layer with the patches can be seen in Fig. 5. Holes were made in the metallic plate to pass the two coaxials of each array element to the lower face of the plate. At the other end both probes are connected to the inputs of a 3 dB-90° hybrid. The substrate employed in this case is Epsilam ($\epsilon_r = 10.5$) of thickness 0.635 mm. LIBRA-Series IV software of HP-EESOF was used for the design of the hybrid. The output of the hybrid is connected to a monolithic LNA. Both the hybrid and the LNA are mounted on a carrier screw onto the lower face of the antenna, as shown in Fig. 6.

The whole array was measured in an anechoic chamber. A comparison between the simulated and measured radiation patterns at the output of six-way combiner are shown in Section II-B1.

3) Monolithic Low Noise Amplifier: The monolithic low noise amplifier (LNA) is a two-stage circuit based on MESFET's with input, output and interstage LC lumped matching networks. The first stage determines the total noise figure of the amplifier. Minimum noise and maximum gain usually require different input networks. Inductive series feedback in a common source configuration is employed in this stage to achieve low noise figure and good input matching simultaneously [15]. For the second stage, RC feedback is used to improve stability in the band dc-20 GHz and to increase the gain of the whole amplifier without modifying the noise figure because of the high gain of the previous stage ($G > 10$ dB). The LC matching networks are also used to bias the circuit in order to reduce the number of spiral inductors, which allows a reduction in chip size.

Monolithic spiral inductors with large inductance values are necessary in L-band MMIC's if LC matching elements are required. Since a spiral inductor needs a high number of turns with a long line length to increase the inductance value, the parasitic elements are large and adversely affect the MMIC performance.

The LNA was designed using LIBRA_Series IV of HP-EESOF and was fabricated at the GEC-Marconi Foundry using their standard 0.5 μm MESFET F20 process. A photograph of the chip with 2×2 mm^2 size is shown in Fig. 7(b). The performance can be summarized as follows. At the central frequency (1.575 GHz) the gain is higher than 25 dB and the noise figure is less than 2.3 dB. In a 250 MHz band centered at 1.575 GHz, the input and output matching are better than -10 dB, the gain is better than 23 dB and the noise figure is less than 2.7 dB, as is shown in Fig. 7(a). The noise figure of the amplifier is determined by losses on the input matching networks at low frequencies and by the device performance as the frequency increases. The parasitic resistance of the inductor in the input matching network has a large influence on the MMIC noise performance due to its inherent losses. This explains the noise figure versus frequency characteristics of the LNA in Fig. 7(a). The power consumption is 60 mW (3 V–20 mA).

B. RF Receiver Architecture

1) RF Channel: The signal from each element of the array antenna is applied to the RF subsystem, where beam conformation is done. The head of this RF subsystem consists of six identical channels, each one including a 3 dB-90° hybrid and the silicon monolithic IC HPMX2001 from Hewlett-Packard [16]. The signal outputs are added in a six-way microstrip combiner [17]. All circuits have been designed in hybrid technology. A photograph of this subsystem is shown in Fig. 8. The IC HPMX2001 is a quadrature phase shift keyed (QPSK) modulator which consists of two double balanced mixers, an adding circuit to combine the outputs and output amplifier. The topology selected for the mixer is the Gilbert Cell balanced modulator. The typical LO operating frequency range of this device is from dc-2000 MHz, which makes it very useful in L-band applications.

Although the use of analogic devices as vector modulators to provide an accurate phase shift at constant amplitude for different attenuation levels, have been proposed for adaptive array antennas and multifunction microwave communication systems [18], it is the first time a low cost device has been used to implement a vector control function. It is a key element of this design. The other key element is a control board, specifically designed for this application, through which it is possible to do a sensitive control of the dc signals for channels I and Q using the software described below. Fig. 9 shows a

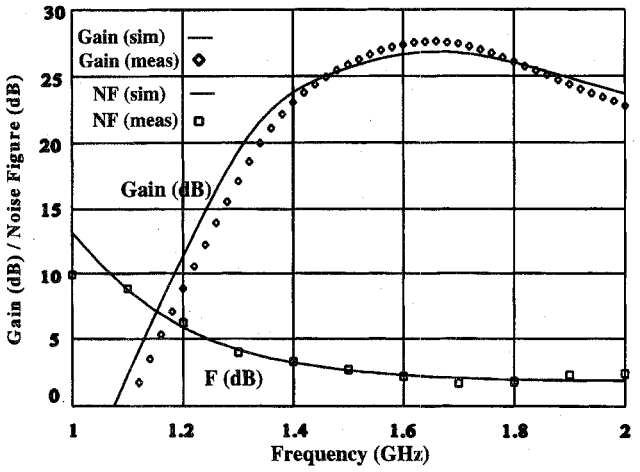

(a)

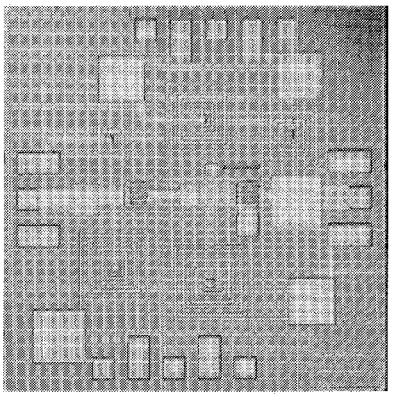

(b)

Fig. 7. (a) Gain and noise figure of monolithic LNA. (b) Chip photograph.

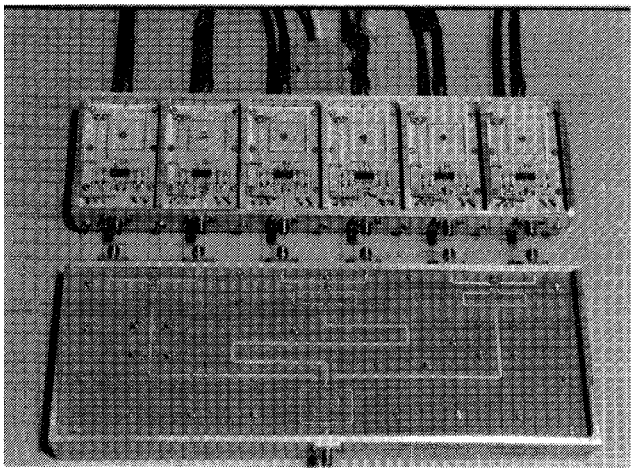

Fig. 8. Photograph of 6 QPSK modulators and combiner network.

functional block diagram of the design, including the digital control and RF portions of the circuit. This merger of RF and digital technology provides good electrical performance at a competitive cost.

Next, a brief description of the techniques used for error correction and control board design is given.

With reference to Fig. 9, the RF signal is fed to a 3 dB-90° hybrid which provides two RF input signals in quadrature necessary for the vector modulator. The Gilbert Cell modulators of HPMX2001 take the RF input signals and the dc control signals from I' and Q' channels and create the output signals, which are modified both in amplitude and phase. If the input signal is represented as $x(t) = A\sin(\omega t)$ (taking null phase as reference), the output signal will be given by:

$$y(t) = II'\sin(\omega t) + QQ'\sin(\omega t + \phi) \tag{1}$$

where I designates the amplitude of the in-phase channel, Q the amplitude of the quadrature channel, ϕ is the phase difference between I and Q (ideally 90°), and I' and Q' represent the amplitude of the dc control signals. Supposing that no errors are present in the system at the design frequency, which means that the I and Q channels have the same amplitude and $\phi = -90°$, the amplitude and phase of the output signal will be given by

$$\text{Amplitude} = \frac{A}{\sqrt{2}}\sqrt{I'^2 + Q'^2}$$
$$\text{Phase} = \tan^{-1}\frac{I'}{Q'}. \tag{2}$$

It is clear that if θ_n is the phase shift and k_n is the attenuation (in dB) needed in the n-th element of the array ($n = 1 \cdots 6$) to set the desired radiation pattern, the required values for the I'_n and Q'_n levels in this channel can be calculated as follows [19]

$$I'_n = 10^{k_n/20}\sin(\theta_n), \quad Q'_n = -10^{k_n/20}\cos(\theta_n). \tag{3}$$

In the present design, these dc voltages must have a maximum excursion less than ±1 V, to avoid the saturation in the mixers and must be centered at 2.5 V. However, in a practical situation, an amplitude and phase unbalance will be present in both, hybrid coupler and Gilbert cell-mixers in the IC. As a consequence of these errors the output amplitude and phase shift will be dependent on the output RF signal phase. In fact, the output signal in a phase sweep from 0 to 360° will describe an ellipse instead of a circle if no compensation is applied, as can be seen in Fig. 10.

In this figure, the phase relationship between I-Q components of the output signal in a bandwidth of 2 MHz, in two different situations, is shown. When the amplitude and balance error on phase are uncompensated, and when the I' and Q' control signals are modified to correct the previous error. This is the great advantage of this control system, since test measurements can be quickly done under all working conditions. The errors can be corrected introducing two parameters, the global amplitude error k_{err}, which represents the amplitude imbalance between the channels I and Q, and α_{err}, which represents the phase difference from the ideal value. So it is considered that

$$I = k_{\text{err}}Q$$
$$\phi = -90° + \alpha_{\text{err}}. \tag{4}$$

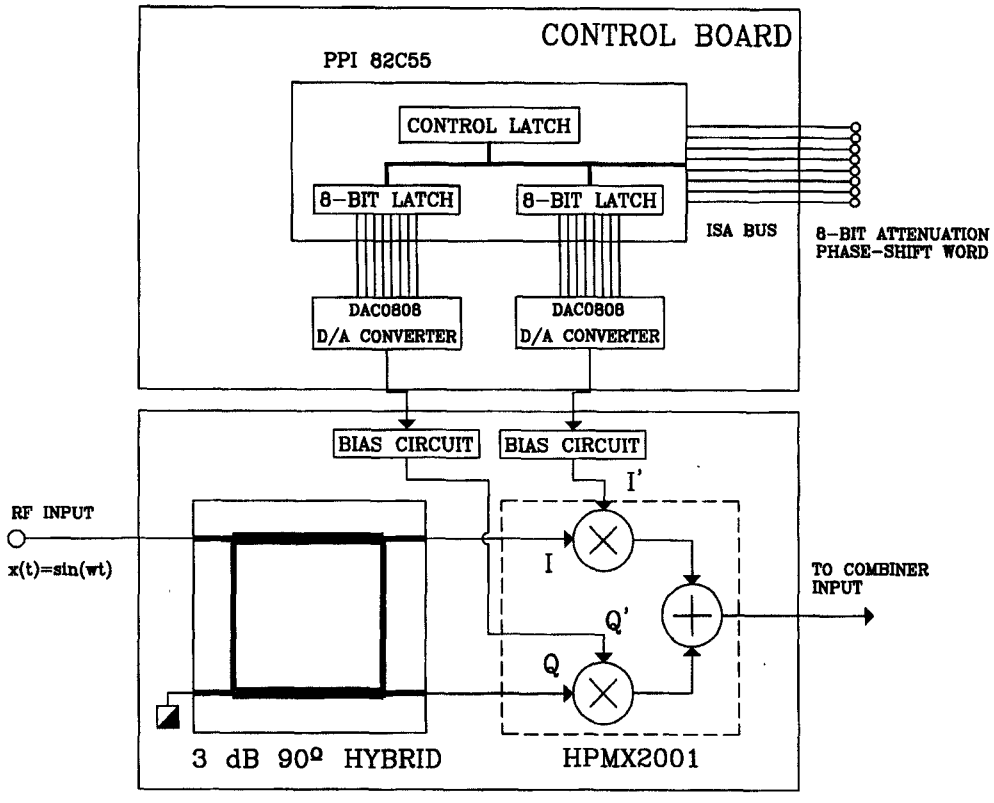

Fig. 9. Block diagram of vector modulator and control boards.

Introducing this values in (1) and operating, the output signal $y(t)$ is then given by

$$y(t) = \frac{A}{\sqrt{2}}[k_{\text{err}} I' - Q' \sin(\alpha_{\text{err}})] \sin(\omega t) - \frac{A}{\sqrt{2}}[Q' \cos(\alpha_{\text{err}})] \cos(\omega t) \quad (5)$$

and now the values for the control signals I'_n and Q'_n can be recalculated as

$$I'_n = \frac{k_{1n}}{k_{\text{err}}}[\cos(\theta_n) \tan(\alpha_{\text{err}}) + \sin(\theta_n)] \quad (6)$$

$$Q'_n = -\frac{k_{1n} \cos(\theta_n)}{\cos(\alpha_{\text{err}})} \quad (7)$$

with results as shown in (8) at the bottom of the page, where k_n and θ_n are the desired attenuation and phase values respectively, as in the ideal case. The values for k_{err} and α_{err} can be found experimentally, making a measurement of the six RF channels at the design frequency. The amplitude variation obtained at the output depends on the needed attenuation, due to the discrete values provided by the D/A converter and the bias adjustment applied. At 0 dB attenuation this value is only ± 0.1 dB. Fig. 11 shows the amplitude variation is shown for different attenuation values. The variation in phase is always included between $\pm 1°$ for a 0 dB attenuation value, and $\pm 5°$ for 20 dB. This value of 20 dB in the attenuation will be considered the practical working limit. This developed correction technique can be successfully applied in a wide range of frequencies. In fact, a bandwidth greater than 250 MHz can be obtained although the 3 dB-90° hybrid is a narrow band element.

The other key element of the design is the control board. It allows the setting of the desired attenuation and phase shift values by the two dc control signals applied to I' and Q' channels. Each one of these dc signals is obtained through an 8 bit D/A converter associated to a latch register, in order to maintain the values once they have been supplied. The 12 registers and D/A converters needed in total for the six channels are grouped into two PC boards, as a versatile control system which can be easily handled by software. The DAC0800 converters and the Programmable Peripheral Interface (PPI) 82C55A have been used. This last IC is a general purpose programable I/O device designed for use with iAPX family microprocessor, containing three 8-bit ports that can be configured by software in a wide variety of functional characteristics.

$$k_{1n} = \frac{10^{k_n/20}}{\sqrt{[\cos(\theta_n) \tan(\alpha_{\text{err}}) + \sin(\theta_n)]^2 + \dfrac{\cos^2(\theta_n)}{\cos^2(\alpha_{\text{err}})} - 2[\cos(\theta_n) \tan(\alpha_{\text{err}}) + \sin(\theta_n)] \cos(\theta_n) \tan(\alpha_{\text{err}})}} \quad (8)$$

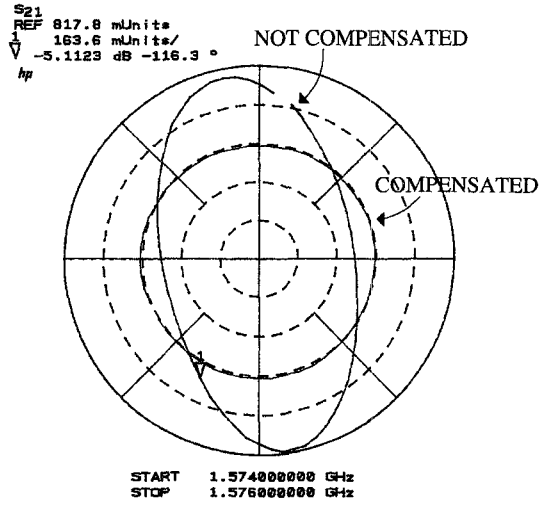

Fig. 10. Amplitude response in a phase sweep at 0 dB attenuation.

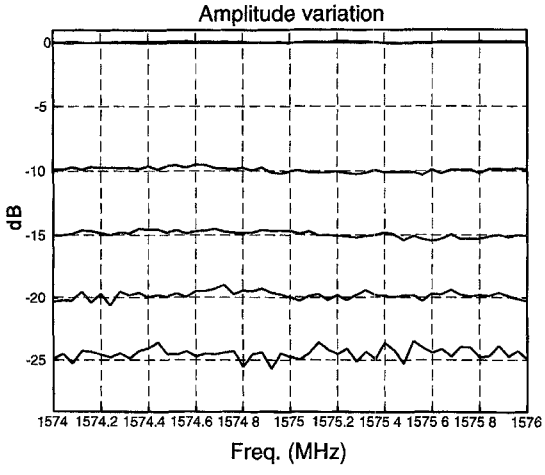

Fig. 11. Amplitude variation for different attenuation levels.

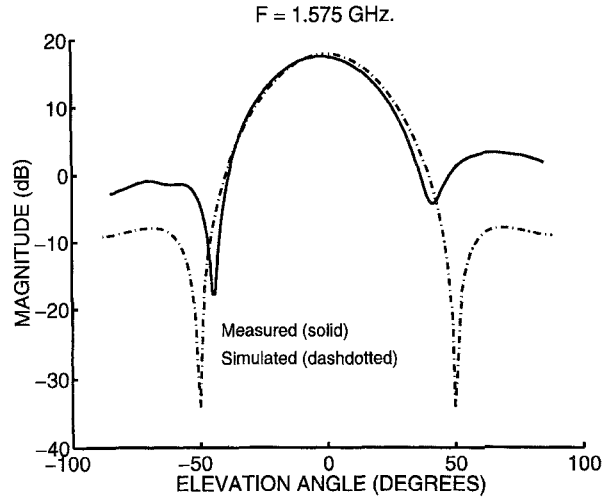

Fig. 12. Radiation pattern of antenna system at broadside (Azimuth = 30°).

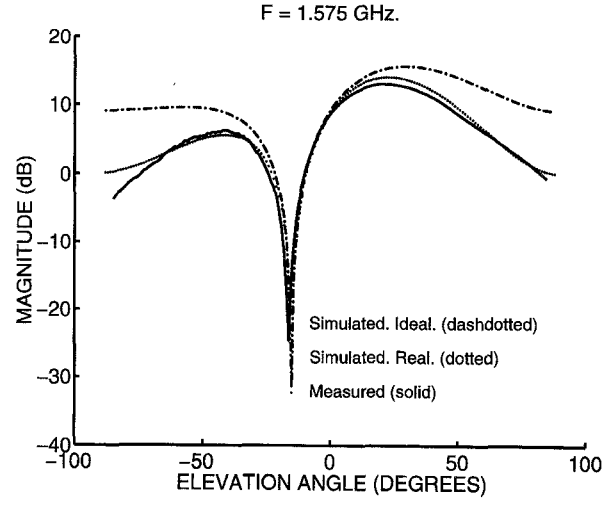

Fig. 13. Radiation pattern of antenna system at elevation = 60° and azimuth = 60°.

The six output signals of each RF channel are added by a six-way microstrip combiner. Its output will be the RF signal that will be processed in the GPS receiver, as is described later. A balance of 0.5 dB in amplitude and 1.5° in phase for all inputs was obtained. In this element only the amplitude error will have some kind of influence, because the phase errors will be automatically corrected in a subsequent calibration process.

The antenna system can be characterized by measuring the radiation patterns in an anechoic chamber at the output of the RF subsystem, thus including the vector modulators and the combiner described above. Two significant cases are presented in Figs. 12 and 13. The curves have been normalized with respect to one of the antenna elements pattern. The first figure corresponds to the array looking at broadside where it can be observed that the sidelobes are 15 dB below the main beam and the $\theta_{3\text{dB}}$ beamwidth is the $\pm 17°$ as expected from a six elements circular array. Fig. 13 is obtained with the array looking at an elevation angle of 60° and an azimuth angle of 60° by controlling the six phase-shifters. The weights applied to each element array were obtained assuming ideal elements. Note that the maximum is not at 30° from broadside but at 22°. This is due to the directivity of the array elements. Also the simulations of the array factor are included in figure to show this effect. One case considers ideal elements (isotropic) and the other real elements (modeled as two magnetic currents separated $\lambda_g/2$). It can be seen how the measured curve fits the simulated array factor considering real elements where the maximum effectively occurs at an angle of 22° from broadside, while the array factor with ideal elements also shown in the figure has the maximum at 30° from broadside, as expected.

2) GPS Receiver: Use of commercial application specific integrated circuits (ASIC's) for receiver design and building makes possible frequency downconversion, filtering and A/D signal conversion for further processing. This provides a receiver giving very good performances at a low cost, useful for algorithm development and testing in mobile communications environments. The fact of being a GPS receiver has the advantage of the system capabilities for calibration and tracking algorithms, being the conclusions of general character, so as to be applied to others systems.

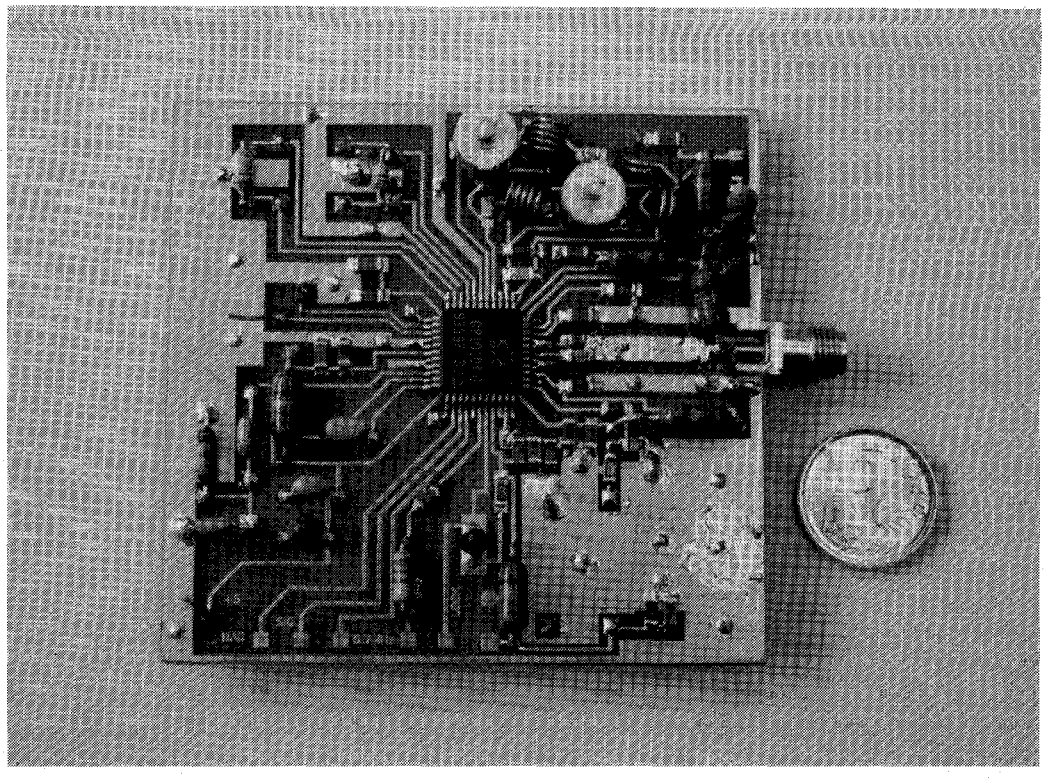

(a)

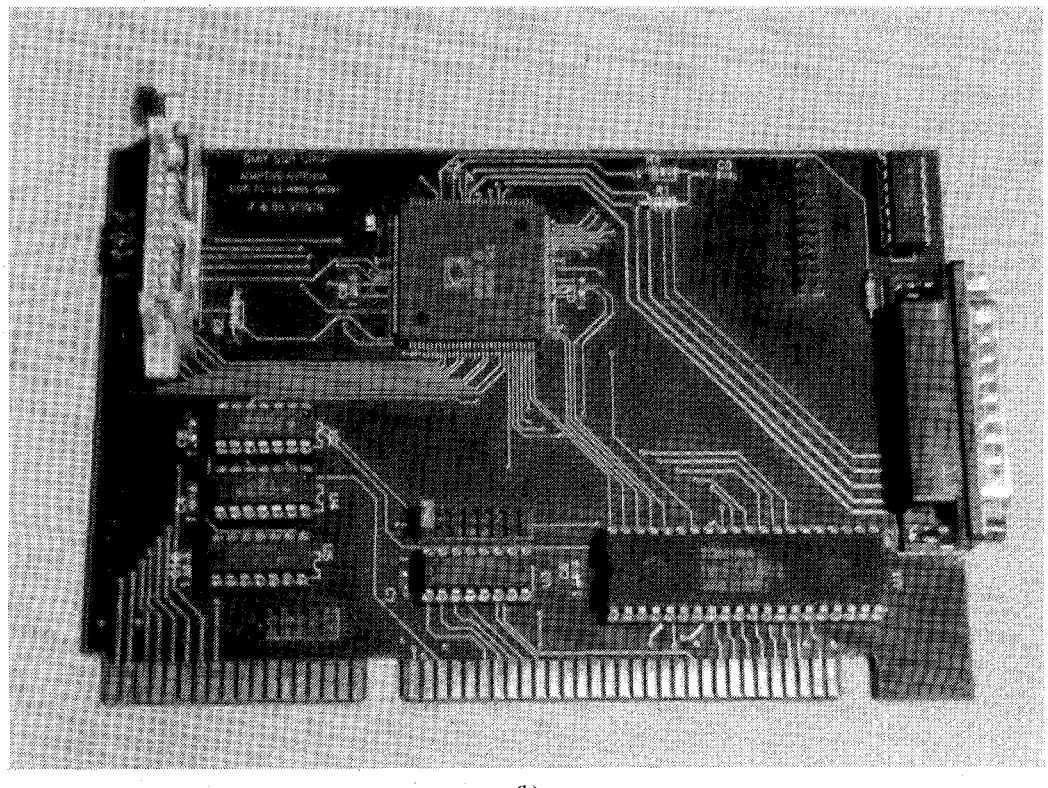

(b)

Fig. 14. GPS receiver. (a) GP1010 GPS receiver front-end. (b) GP1020 six-channel digital correlator.

The GPS system provides accurate information on the user's position and speed and a very accurate time reference. The GPS satellites transmit a signal centered at 1.575 GHz that carries a 50 bauds bit rate and is spread by a Pseudo Random Noise (PRN) code at 1.023 MChip/s. The movement of the satellites produces unknown doppler shift and a delay in the envelope of the signal at the receiver. Therefore, the receiver should be able to overcome these two difficulties: compensate

the doppler frequency (up to 10 KHz peak to peak) and to synchronize the internally generated code with the code actually received.

As we know, the GPS system provides accurate information on the user's position and spreads a very accurate time reference.

Two commercial ASIC's, the GP1010 and GP1020 from Plessey Semiconductors [20], [21], are used in the implementation of the hardware. The first one downconverts the input frequency in three stages to get an IF signal centered at 4.32 MHz. The output of the last mixer is sampled at 5.71 MHz and coded with only 2 bits. The second ASIC, a six-channel parallel correlator, accomplishes the following tasks: down conversion to base band, with the needed doppler cancellation, the decorrelation or matched filtering with the code corresponding to each satellite, bit synchronization and decision on the symbol of the BPSK constellation.

All the digital signal processing involved is guided by a low cost microprocessor. The microprocessor serves the second integrated circuit asynchronously. The rest of the tasks are carried out by the microprocessor. They comprise the estimation of the satellite-user distance, acquisition of the universal coordinated time (UCT), decoding of the navigation message sent by the satellites and the computation of the users location. In addition to the mentioned tasks, the microprocessor has to control the digital ASIC. This architecture of the receiver allows a great flexibility and robustness.

Since the length of the PRN code for all the GPS satellites is the same and equal to 1 ms, the receiver computes the difference between the received chips that match the code replica generated at the receiver and the ones that do not match along 1 ms. Because the front-end of the receiver incorporates an automatic gain control (AGC) the power of the signal (signal of interest plus interferences plus noise) crossing the IF stage is almost constant, and therefore the amplitude at the output of the decorrelator is proportional to the SNR, which is available once every millisecond. This SNR measurement rate allows the algorithms in following stages to update the weight vector fast enough to handle wireless mobile communications environments.

Fig. 14 is a picture of the two commercial ASIC's used to implement the GPS receiver.

III. Calibration and Tracking Algorithms

A. Calibration Algorithm

In order to get the system working properly, a previous calibration is needed. The calibration facility allows the system to know both the receiver orientation and the manufacturing differences between the six RF channels. For this process, a technique using GPS satellites has been developed, with good results in practice.

In this method the assumption that the carrying vehicle is not tilted is made, in order to reduce unknown parameters. The first step chooses two satellites, say S_1 and S_2, placed at a medium elevation and a quite different azimuth, and optimizes phase shifts with a blind algorithm, which consist of doing a phase sweep in each RF channel, taking one of them as a reference, until a maximum of SNR is obtained. Two sets of six actual shifts, called $\boldsymbol{A_{S_1}}$ and $\boldsymbol{A_{S_2}}$ are obtained. Afterwards, it is supposed that the heading of the array is zero degrees, and phase shifts are theoretically calculated, using the position given by the satellites in their navigation message, for both satellites, say $\boldsymbol{T_{S_1}}$ and $\boldsymbol{T_{S_2}}$. The differences between actual and theoretical shifts are called corrections, $\boldsymbol{C_{S_1}} = \boldsymbol{A_{S_1}} - \boldsymbol{T_{S_1}}$ and $\boldsymbol{C_{S_2}} = \boldsymbol{A_{S_2}} - \boldsymbol{T_{S_2}}$, and should be equal to the shifts introduced by the different components of the RF channel, if the supposed heading was correct. Note that actual values do not depend on the supposed bearing of the array, since they are experimental, and so it is only needed to recalculate the theoretical values, $\boldsymbol{T_{S_1}}$ and $\boldsymbol{T_{S_2}}$, for new heading assumptions until $\boldsymbol{C_{S_1}}$ and $\boldsymbol{C_{S_2}}$ are the same. In this case, any of these subsets represents the actual shifts of the components of every RF channel.

B. Control and Processing Software

The PC is provided with specifically developed software applications allowing the whole system to be controlled, tested, and simulated. Simulation is used as a first check when developing new algorithms, giving an idea of the predicted system behavior before running real time control programs. It is also helpful to evaluate the actual results obtained and to determine why they match or not with the expected ones. The control software can work in manual and automatic modes. The manual mode asks the user for the phase shifts and attenuations he wants applied to the channels. According to these values, any possible radiation diagram can be used. The simulation software includes a tool to look at the expected shape of these diagrams before the manual introduction of the values into the real system.

There are some automatically performed functions: searching, tracking, position parameters determination and autocalibration. New facilities for unwanted signals adaptive cancellation are being developed.

When the system is turned on, an automatic search is made, aimed at determining a desired satellite position. The vertical beamwidth (3 dB) is large (about 60°, making it possible to determine the satellite azimuth in just an azimuthal sweep, with steady beam elevation of 50°; once this operation has been performed, a pseudomonopulse operation [22], pointing beams to 0 and 90°, allows the elevation to be found in the following manner: the monopulse function is calculated, and the offset angle is derived given that the relation between the monopulse function and angle is known. This is given simply by knowing the slope of this relation. In order to have a precise elevation value, this monopulse function slope has been theoretically calculated, and successfully applied to the system.

The tracking facility works on a pseudomonopulse basis [22]. After a first satellite position is obtained, the main beam is pointed to its right and later to its left, so with both signal levels the monopulse function is calculated. Since the slope of this function is know, the offset angle is easily calculated and so the satellite azimuth is predicted. Since the environment is noisy, as some other GPS satellites introduce their own

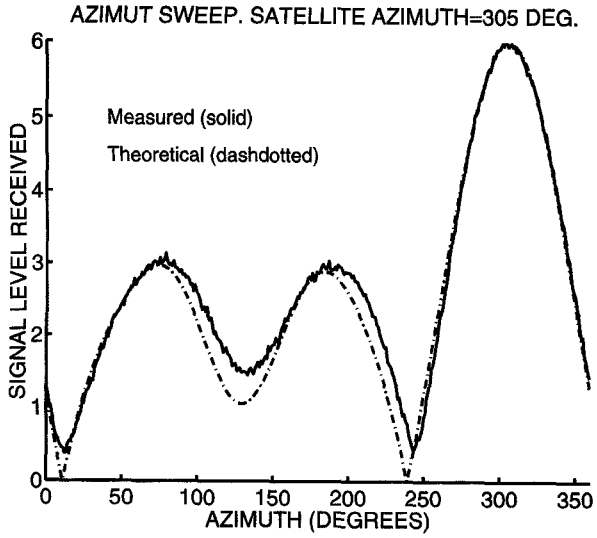

Fig. 15. Complete azimuthal scanning.

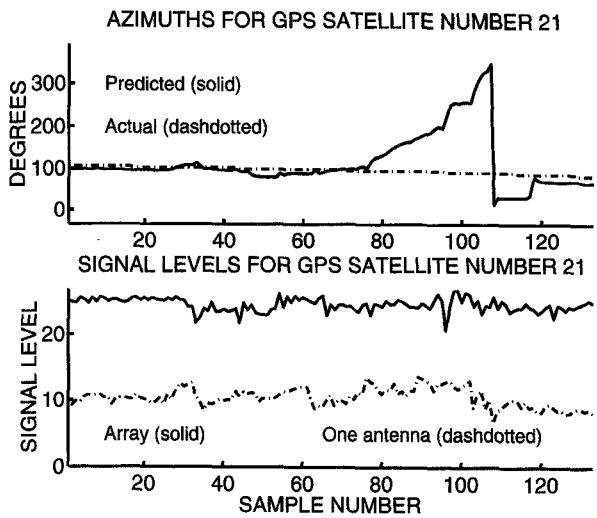

Fig. 16. Azimuths and signal levels while tracking.

signals into the receiver correlator, a final recursive filtering is performed, and the position is determined. While this process is repeated, the satellite is tracked.

Position parameters, heading, and tilting of the carrying vehicle, are determined if the tracked satellite position is known. This is attained by looking at the computer register where the azimuth and elevation pointing angles are stored. The difference between these last and the actual azimuth and elevation angles determine the azimuth and elevation offsets from the zero degrees heading and elevation. Normally, the carrying vehicle stands on a planar surface and tilting is not a problem; but normally azimuthal angles are always changing.

Autocalibration consists of determining the phase shifts introduced by the RF channels. At the nominal frequency (1575 GHz), any component manufacturing difference introduces an important phase shift to be taken into account. This problem comes again when an antenna or cable substitution is needed. The calibration facility lets these shifts be determined automatically, as explained in previous section.

Figs. 15 and 16 give an idea of the experimental results obtained. A good way of testing the system is to make an azimuthal sweep at steady elevation. If the satellite being currently tracked is located at the position expected from the values got while tracking, a maximum should be obtained exactly when the steady elevation sweep passes through the satellite azimuth. This situation has been reproduced and the values are depicted in Fig. 15. As can be seen, the system response matches almost exactly the actual position of the satellite, as given by the GPS receiver.

Some tracking tests have been performed. The whole system was loaded into a car, using the metallic roof as the ground plane of the array. Fig. 16 shows the results obtained for a given trajectory of the car in a very low traffic track. The upper graph contains the tracked satellite azimuth (dashdotted line), as given by the GPS receiver, and the satellite azimuth estimated by the system (solid line). Note that when the car turns, the own system is not aware of that, and acts like if the surrounding scenario (including the tracked satellite) was turning. In this case, the changes in the predicted azimuth should be just the opposite of what the car does. For obtaining the data of Fig. 16, the car began to run straight (samples 0–25); then the car simulated an overtaking, going to the left (26–35), and back to the right lane (45–55). After a few meters, a 360° turn was made according to the following sequence: smooth curve (samples 76–95), sharp curve (95–98), stop (99–103), sharp curve (104–110), stop (111–118), and sharp curve up to the initial orientation of the car. The lower graph depicts the signal levels (logarithmic units) obtained while tracking in the same test, for the whole array pointed to the predicted satellite position (solid line) and only an antenna (dash-dotted line). The difference between both lines gives an idea of the improvement obtained when using the electronically steered array instead of only an antenna. Furthermore, the plot for the whole array keeps similar values for all the samples taken, which is an indication of a correct tracking, independently of the relative position between satellite and carrying vehicle.

IV. Conclusion

In this paper the design and basic characteristics of an electronically steered adaptive array antenna for land vehicle operation are described. The aim with the reported antenna has been to obtain a system allowing the performance of experiments in order to evaluate a possible solution to the mobile antenna segment of a mobile satellite communication system. The work involved in the planar array and RF subsystem design, the use of commercial and low cost components, the calibration process and the developed tracking algorithms have been described and some field tests have been reported.

Acknowledgment

The authors would like to thank V. Mauer for his useful suggestions and comments in the design of the GPS receiver.

References

[1] W. W. Wu, E. F. Miller, W. L. Pritchard, and R. L. Pickholtz, "Mobile satellite communications," *Proc. IEEE*, vol. 82, pp. 1431–1448, Sept. 1994.

[2] A. C. Densmore and V. Jamnejad, "A satellite-tracking K and K_a-band mobile vehicle antenna system," *IEEE Trans. Veh. Technol.*, vol. 42, pp. 502–513, Nov. 1993.
[3] P. V. Brenan, "Low cost phased array antenna for land-mobile satcom applications," *IEEE Proc.-H*, vol. 138, no. 2, pp. 131–136, Apr. 1991.
[4] U. Forssén *et al.*, "Adaptive arrays for GSM900/DCS1800," in *Proc. 44th. IEEE Veh. Technol. Conf.*, June 1994, pp. 605–609.
[5] H. Anderson, M. Landing, A. Rydberg, and T. Oberg, "An adaptive antenna for the NMT900 mobile telephony system," in *Proc. 44th. IEEE Veh. Technol. Conf.*, June 1994, pp. 610–614.
[6] R. Telikepalli *et al.*, "Wide band microstrip phased array for mobile satellite communications," *IEEE Trans. Microwave Theory Tech.*, vol. 43, pp. 1758–1763, July 1995.
[7] K. R. Carver and J. W. Mink, "Microstrip antenna technology," *IEEE Trans. Antennas Propagat.*, vol. 29, pp. 2–24, Jan. 1981.
[8] D. M. Pozar, "Microstrip antennas," *Proc. IEEE*, vol. 80, pp. 79–91, Jan. 1992.
[9] Q. Song and X.-X. Zhang, "A study on wideband gap-coupled microstrip antenna arrays," *IEEE Trans. Antennas Propagat.*, vol. 43, pp. 313–317, Mar. 1995.
[10] J. T. Aberle, D. M. Pozar, and J. Manges, "Phased arrays of probe-fed stacked microstrip patches," *IEEE Trans. Antennas Propagat.*, vol. 42, pp. 920–927, July 1994.
[11] G. G. Gentili, L. E. García, F. Pérez, and M. Salazar, "Efficient Green's function analysis of stacked microstrip patch antennas residing in a cavity," *Workshop Syst. Applicat. Integrated Antennas*, 25th Europe. Microwave Conf., Workshop Proc., Bologna, Italy, Sept. 1995, pp. 105–110.
[12] R. J. Mailloux, "On the use of metallized cavities in printed slot arrays with dielectric substrates," *IEEE Trans. Antennas Propagat.*, vol. 35, pp. 477–487, May 1987.
[13] D. M. Pozar and D. H. Schaubert, "Scan blindness in infinite phased arrays of printed dipoles," *IEEE Trans. Antennas Propagat.*, vol. 32, pp. 602–610, June 1984.
[14] G. G. Gentili, L. E. García, F. Pérez, and M. Salazar, "Green function analysis of single and stacked rectangular microstrip patch antennas enclosed in a cavity," to be published in *IEEE Trans. Antennas Propagat.*
[15] Y. Imai, M. Tokumitsu, and A. Minakawa, "Design and performance of low-current GaAs MMIC's for L-band front-end applications," *IEEE Trans. Microwave Theory Tech.*, vol. 39, pp. 209–214, Feb. 1991.
[16] Hewlett-Packard, "Communications components," *GeAs and Silicon Products Designer's Catalog*, ch. 8, pp. 7–12, 1993.
[17] A. A. Saleh, "Planar electrically symmetric n-way hybrid powers/combiners," *IEEE Trans. Microwave Theory Tech.*, vol. MTT–28, pp. 555–563, June 1980.
[18] S. Lucyszyn and J. D. Robertson, "Vector modulators for adaptive and multi-function microwave communication system," in *Proc. Microwaves 94*, Oct. 1994, pp. 103–105.
[19] M. Tuckman, "I-Q vector modulator—The ideal control component?," *Microwaves Syst. News*, pp. 105–115, May 1988.
[20] GP1010, *Global Positioning Receiver Front-End*, GEC Plessey Semicond., Data Sheets, Apr. 1994.
[21] ——, *Six-Channel Parallel Correlator Circuit GPS or GLONASS Receivers*, GEC Plessey Semicond., Data Sheets, Feb. 1994.
[22] S. M. Sherman, *Monopulse Principles and Techniques*. Dedham, MA: Artech House, 1985.

José I. Alonso (M'90) was born in Villacañas, Toledo, Spain. He received the degree in telecommunication engineering in 1982 and the Ph.D. degree in 1989, both from the Polytechnic University of Madrid, Spain.

From 1982 to 1985 he worked as a Microwave Design Engineer at Telettra España S.A. (Alcatel Standard S.A.). In 1985 he joined the Signal, System and Radiocommunications Department at the Technical School of Telecommunication Engineering, where he is currently Associate Professor. His research is concerned with computer-aided design of high-speed/high frequency integrated circuits and their interconnections. In addition, he has been engaged in research and development of GaAs monolithic microwave integrated circuits (MMIC's) and their applications to mobile, satellite and optical-fiber communication systems.

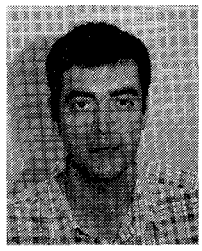

José M. Blas was born in Cuenca, Spain, in 1967. He received the B.S. and M.S. degrees in 1992 and 1993, respectively, from the Polytechnic University of Madrid, Madrid, Spain.

He is with the Department of Signals, Systems, and Radiocommunications, Polytechnic University of Madrid, where he is pursuing the Ph.D. degree. His research activity and interest are in GaAs monolithic microwave integrated circuits (MMIC's), and their applications to satellite mobile communications.

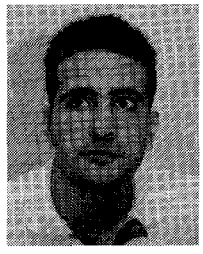

Luis E. García (S'96) was born in Madrid, Spain, in 1967. He received the B.S. and M.S. degrees in 1991 and 1992, respectively, from the Polytechnic University of Madrid.

He is with the Department of Signals, Systems, and Radiocommunication, Polytechnic University of Madrid, where he is pursuing the Ph.D. degree. His research activity and interest are in the area of applications of numerical methods, mainly the finite elements, to electromagnetic problems.

Javier Ramos (S'96) was born in Madrid, Spain, in 1966. He received the degree in telecommunication engineering in 1992 and the Ph.D. degree in 1995, both from the Polytechnic University of Madrid.

He is currently a Scientific Visitor at Purdue University, West Lafayette, IN. His research activities involve GPS applications, array signal processing, and CAD for system simulation.

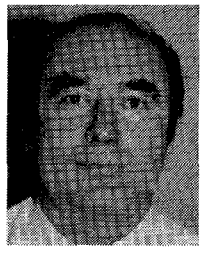

Jesús de Pablos was born in Pamplona, Spain, in 1956. He received the degree in telecommunication engineering in 1980 from the Polytechnic University of Madrid, Madrid, Spain.

After working in computers from 1981 to 1983 and electronics from 1984 to 1986, he joined the Polytechnic University of Madrid in 1987, where he teaches courses in electronics and communications as Professor at the Technical School of Aeronautic Engineering. He is also developing tracking algorithms in close relationship with the Department of Signals, Systems, and Radiocommunications, Technical School of Telecommunication Engineering.

Jesús Grajal was born in Toral de los Guzmanes, León, Spain, in 1967. He received the degree in telecommunication engineering in 1992 from the Polytechnic University of Madrid, Madrid, Spain.

He is with the Department of Signals, Systems, and Radiocommunications, Polytechnic University of Madrid, where he is pursuing the Ph.D. degree. His research activities are high frequency circuit and system design, both in hybrid and monolithic technology, and semiconductor device simulation as well.

Gian G. Gentili (M'96) was born in Turin, Italy. He received the "laurea" degree in electronic engineering from Politecnico di Milano, Milano, Italy, in 1987.

From 1987 to 1989, he was with Politecnico di Milano as a scholarship holder, developing CAD tools for electromagnetic analysis of microstrip circuits. In 1989, as a Researcher, he joined the "Centro Studi sulle Telecomunicazioni Spaziali" (CSTS-CNR), which resides at Politecnico di Milano. Since then, he has worked on the application of numerical methods for the modeling and design of microwave and millimeter wave passive structures.

Javier Gismero was born in Madrid, Spain. He received the degree in telecommunication engineering in 1984 and the Ph.D. degree in 1989, both from the Polytechnic University of Madrid, Spain.

In 1985 he joined the Department of Signals, Systems, and Radiocommunications, Polytechnic University of Madrid, where he is currently Associate Professor. His research activity involves high frequency circuits and systems design, both in hybrid and monolithic technology.

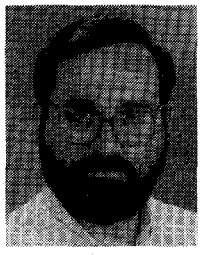

Félix Pérez (M'96) was born in Castejón, Spain, in 1954. He received the degree in telecommunication engineering in 1977 and the Ph.D. degree in 1982, both from the Polytechnic University of Madrid, Spain.

From 1978 to 1987 he has been at the Department of Microwaves, Polytechnic University of Madrid, first as Assistant Lecturer and then as Associate Professor. He is presently Professor in the Department of Signals, Systems, and Radiocommunications. His research interests have been mainly in MESFET's, front-ends for DBS-TV, and millimeter wave circuits. He is currently engaged in the development of solid-state radar systems and radar system simulation.